Performance Delivered by All Adaptive Optics Modes in GNAO

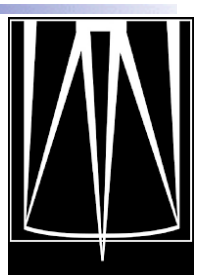

GNAO-SYS-SIM-006

Related PBS ID: 5.2

M. van Dam, G. Sivo

June 12, 2020

Contents

1 Introduction....4
2 Observing modes....4
2.1 Multi-conjugate adaptive optics....4
2.2 Ground-layer adaptive optics....5
2.3 Laser tomography adaptive optics....5
2.4 Single conjugate adaptive optics....5
3 Simulation parameters....5
3.1 Guide star locations....5
3.2 Atmospheric parameters....5
3.3 Sodium return and Rayleigh....5
3.4 Optical throughput....6
3.5 LGS WFS camera....6
3.6 NGS WFS Camera....6
3.7 Windshake and vibrations....7
3.8 Deformable mirror characteristics....7
3.9 M2 print-through....7
3.10 Science metrics....7
4 Simulation description and results....8
4.1 Simulation tool....8
4.2 Simulation results summary....8
4.3 Multi-conjugate adaptive optics....10
4.4 Ground-layer adaptive optics....11
4.5 Laser tomographic adaptive optics....13
4.6 Single conjugate adaptive optics (3 NGS)....15
4.7 Single conjugate adaptive optics (1 NGS)....17

Document Acceptance and Release Notice
This document is a managed document. To identify changes, each page contains a release number and a page number. This document is authorized for release once all signatures have been obtained.

APPROVED:	*Approval on file* William Rambold GNAO Project Lead Systems Engineer	Date:	10/21/20
APPROVED:	*Approval on file* Manuel Lazo GNAO Project Manager	Date:	10/21/20
APPROVED:	*Approval on file* Gaetano Sivo GNAO Principal Investigator	Date:	10/22/20
APPROVED:	*Approval on file* Henry Roe GNAO Sponsor, Gemini Deputy Director	Date:	10/21/20

Change Record

Version	Date	Description	Owner Name	Change Request
1.0	10/28/20	Released through formal change control process	M. van Dam	GEM-97

1 Introduction

The Gemini North Adaptive Optics (GNAO) instrument is a next generation multi-conjugate adaptive optics (MCAO) system designed for a wide range of science cases. The aim is to produce

near diffraction-limited image quality for J-, H- and K-bands. The corrected light is fed to the Gemini Infrared Multi-Object Spectrograph (GIRMOS), which consists of a wide field imager and a number of integral field units (IFUs), each housing a spectrograph. Each IFUs has a dedicated DM on its path to further reduce the wavefront error.

In addition to regular MCAO operation, GNAO can be operated in other observing modes, described in Section 4. In this report, we run end-to-end Monte Carlo simulations to compare the wavefront error delivered to GIRMOS by the different modes. These wavefront errors are converted to point-spread functions (PSFs) and used to compute the Strehl ratio and FWHM over the science field. The effect of of the DM correction within the IFU on the image quality metrics is not included in the analysis.

A more thorough description of the simulations and simulation parameters can be found in previous reports.[1234]

2 Observing modes

2.1 Multi-conjugate adaptive optics

Two lasers are used to produce five side-launched laser guide stars (LGSs), as shown in Figure 1. This configuration has been shown to produce the best performance.[2]

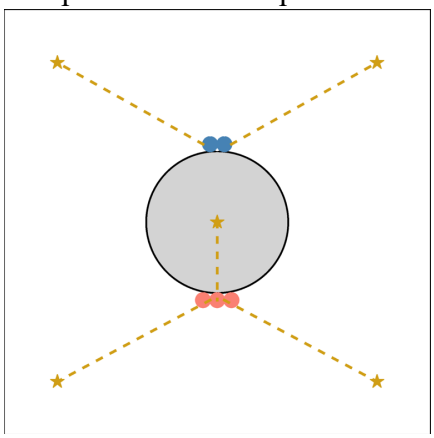

Figure 1: The launch configuration used in this report. The colors of the launch telescope (blue and salmon) represent which of the two lasers is producing the laser light launched by the corresponding launch telescope.

There are five LGS wavefront sensors (WFSs) and three NGS WFSs. The five LGSs are used to drive the three DMs. The signal from the three NGSs is used to drive the tip-tilt mirror and to compensate for tip-tilt anisoplanatism by adding quadratic modes to the high altitude DM(s). This mode delivers the lowest wavefront error over the entire field. The performance is optimized over a 85”x85” square.

2.2 Ground-layer adaptive optics

In ground-layer adaptive optics (GLAO) mode, the five LGSs are used to drive the ground-layer

[1]Marcos van Dam, Gaetano Sivo and Eduardo Marin, “Simulated Performance of GNAO,” GNAO-SYS-SIM-001 v4.0 13 April 2020.
[2]Marcos van Dam, Eduardo Marin, Gaetano Sivo, “GNAO Laser Launch Telescope Location,” v1.0, GNAO-SYS-SIM-003, 11 November 2019.
[3]Marcos van Dam, Gaetano Sivo, Eduardo Marin, “Wavefront Sensor and Deformable Mirror Design Parameters for GNAO,” GNAO-SYS-SIM-004 v3.0 29 April 2020.
[4]Marcos van Dam, Emmanuel Chirre and Gaetano Sivo, “Physical Parameters of Deformable Mirror for GNAO,” GNAO-SYS-SIM-005, v1.0 16 December 2019

DM. The signal from the three NGSs is used to drive the tip-tilt mirror. This mode delivers a much lower level of correction than MCAO, but the performance is uniform over the entire field of view. The performance is optimized over a 85”x85” square.

2.3 Laser tomography adaptive optics

The laser tomography adaptive optics (LTAO) mode uses the same five LGSs and three NGSs to optimize the performance on-axis. By combining the LGS measurements made at different locations in the field, we are able to reduce the effect of focal anisoplanatism, also known as the cone effect. Measurements from the three NGS WFSs are likewise used to estimate the on-axis tip-tilt.

2.4 Single conjugate adaptive optics

A “classical” single conjugate adaptive optics (SCAO) system uses a single on-axis LGS to measure the wavefront. We use the full power of the laser to propagate the single LGS. Classical SCAO systems use a single NGS to measure tip-tilt. The simulations will be run with a single NGS and with three NGSs in order to facilitate the comparison with the LTAO mode.

3 Simulation parameters

In this section, we describe the list of inputs needed to run the simulations.

3.1 Guide star locations

There are five LGS guide stars; one is located at the optical axis [0”, 0”], while the remaining four are located at [±35”, ±35”]. The three NGSs are situated at [0”, 35”], [40”, -30”] and [-40”, -20”].

3.2 Atmospheric parameters

The atmospheric parameters used are the 50th percentile sourced from the TMT (Table 1). The value of r_0 is 0.186 m at 500 nm, while the outer scale is 30 m. Random wind directions were applied to the measured wind speeds. The design parameters will be optimized based on median seeing, and the performance evaluated for all three cases.

Elevation (m)	0	500	1000	2000	4000	8000	16000
Wind speed (m/s)	5.6	5.77	6.25	7.57	13.31	19.06	12.14
Wind direction (°)	190	255	270	350	17	29	66
Turbulence fraction	0.4557	0.1295	0.0442	0.0506	0.1167	0.0926	0.1107

Table 1: Turbulence profile used for Mauna Kea 50th percentile.

The zenith angles simulated are 0º, 25º and 50º.

The dome seeing at Gemini North is believed to be very benign and is ignored in the simulations.

3.3 Sodium return and Rayleigh

Holzlöhner and predicts a return of 14 Mph $m^{-2}s^{-1}$ at the optimal pointing direction with a 20 W TOPTICA laser of which 16 W are launched at the Maunakea site with atmospheric transmission of 0.84.[5] The sodium density for this calculation is $3.75x10^{13}$ atoms m^{-2}.

For Keck II, with a collecting area of 76 m^2, and a 22 W laser, the expected return at the optimal

[5]Holzlöhner R. et al., “Optimization of CW Sodium Laser Guide Star Efficiency,” A&A 510, 0004-6361 January, (2016).

pointing direction is 1.17×10^9. Using the Keck II telescope, the measured return at zenith using a 22 W laser corresponds to the same subaperture intensity in the WFS as an $m_R = 7.5 \pm 0.2$ star.[6] Using a photometric zero point of 1.49×10^{12} photons per second at the top of the telescope for VR-band, this gives 1.48×10^9 photons/second for the telescope, so it is consistent with the expected return.

For Gemini, the collecting area is 48 m^2. Holzlöhner predicts a value of 6.72×10^8 photons/sec for the whole telescope using a 20 W laser. I assumed a value of 3.10×10^8 at the top of the telescope, which is conservative. The reason for this is that other pointing directions can have a factor of two reduction in return, while the sodium density can also vary by a factor of two or more.

In the simulations, we assume that the subapertures contaminated by Rayleigh backscatter will be masked and unused, which is the way that GeMS operates.

3.4 Optical throughput

The optical throughput of the atmosphere is 0.89, the telescope is 0.821, and GNAO is 0.3, for a total of 0.22.

3.5 LGS WFS camera

The baseline detector is an OCAM2 camera, which is based on the CCD220, a 240x240 pixel detector. This is CCD uses electron multiplication, which allows us to get subelectron read noise. The penalty to be paid is the increase in the excess noise factor from 1 to 1.41, which is approximately equivalent to reducing the quantum efficiency of the detector by a factor of 2. The properties of the OCAM2 camera used in the simulations are tabulated in Table 2. The read noise of OCAM2 can be reduced by increasing the multiplication gain, but this ages the camera faster and should be avoided.

Camera	OCAM2
Pixels	240x240
Excess noise	1.41
Quantum efficiency @589 nm	0.90
Read noise	0.5 e-
Dark current	10 e-/s

Table 2: Properties of wavefront sensing cameras used in the simulations obtained from Feautrier *et al*.[7]

3.6 NGS WFS Camera

For the purposes of this report, the three NGS guide stars are assumed to be very bright and the measurement noise is ignored.

3.7 Windshake and vibrations

It is well-known that there are strong vibrations at Gemini North, which have been described

[6]Chin, Jason CY, et al. "Keck II laser guide star AO system and performance with the TOPTICA/MPBC laser." Adaptive Optics Systems V. Vol. 9909. International Society for Optics and Photonics, 2016.

[7]Feautrier, Philippe, et al. "Characterization of OCam and CCD220: the fastest and most sensitive camera to date for AO wavefront sensing." Adaptive Optics Systems II. Vol. 7736. International Society for Optics and Photonics, 2010.

elsewhere. [89] There is a commitment from senior management at Gemini to address this problem. In this study, we we ignore the effect of vibrations.

3.8 Deformable mirror characteristics

The DMs to be used for GNAO have not yet been selected. A description of the properties of the DMs used in the simulations can be found in Table 3.

Parameter	DM1	DM2	DM3
Altitude	0 km	5 km	14 km
Pitch	0.40 m	0.60 m	0.90 m
Actuators across pupil	21	19	19
Coupling	0.15	0.15	0.15
Hysteresis	0	0	0
Stroke	∞	∞	∞
Bad actuators	0	0	0

Table 3: Specification of DM parameters

3.9 M2 print-through

The secondary mirror at Gemini North has a well-known print-through error. The observatory is committed to fixing this problem, so M2 print-through is ignored in these simulations.

3.10 Science metrics

The image quality metrics presented in this report are the Strehl ratio and the Full Width at Half Maximum (FWHM)/ The wavelengths of interest are 1.25, 1.65, 2.2, which corresponds approximately to the central wavelengths of J-, H-, K-bands. The target locations are in a regular grid with positions [-47.4”, -31.6”, -15.8”, 0”, 15.8”, 31.6”, 47.4”] in both x and y, over a circle with a diameter of 2’, as shown in Figure 2.

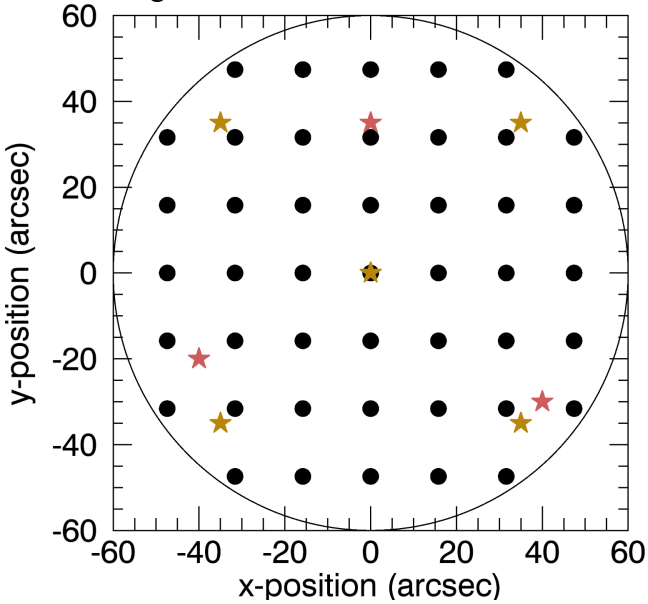

[8]Christou, Julian C., et al. "ALTAIR performance and updates at Gemini North." Adaptive Optics Systems II. Vol. 7736. International Society for Optics and Photonics, 2010.

[9]Lai, Olivier, et al. "Altair performance and upgrades." Adaptive Optics Systems IV. Vol. 9148. International Society for Optics and Photonics, 2014.

Figure 2: Location of science targets (black circles)used to optimize the wavefront correction and to evaluate the image quality. The yellow and red stars represent the LGS and NGS locations respectively.

4 Simulation description and results

4.1 Simulation tool

End-to-end Monte-Carlo simulations were run using YAO,[10-11] an open-source, user-configurable code written in the yorick language, along with custom scripts and parameter files. This code has over 100 users and has been used extensively to design and operate GeMS, the Gemini South MCAO system. A description of the features of the simulations is described extensively elsewhere.[1]

4.2 Simulation results summary

The simulation results are summarized in Tables 4 and 5. The results for each simulation case are plotted in Sections 10 to 17.

[10]Rigaut, François, and Marcos van Dam. "Simulating astronomical adaptive optics systems using Yao." AO4ELT (2013).
[11]http://frigaut.github.io/yao/

	Zenith angle = 0°				Zenith angle = 25°				Zenith angle = 50°			
	Max	Min	Mean	RMS	Max	Min	Mean	RMS	Max	Min	Mean	RMS
MCAO	0.443	0.227	0.340	0.056	0.397	0.175	0.268	0.056	0.205	0.037	0.079	0.037
GLAO	0.139	0.044	0.073	0.021	0.101	0.033	0.054	0.016	0.039	0.016	0.023	0.005
LTAO	0.392	0.027	0.061	0.061	0.370	0.021	0.047	0.056	0.216	0.011	0.021	0.031
SCAO 3	0.339	0.023	0.052	0.053	0.327	0.017	0.040	0.049	0.188	0.010	0.019	0.027
SCAO 1	0.269	0.022	0.049	0.043	0.229	0.017	0.036	0.034	0.224	0.009	0.020	0.032
MCAO	0.623	0.396	0.531	0.056	0.583	0.337	0.460	0.060	0.391	0.124	0.204	0.059
GLAO	0.304	0.098	0.174	0.050	0.259	0.075	0.141	0.043	0.112	0.039	0.060	0.014
LTAO	0.576	0.059	0.144	0.097	0.552	0.047	0.116	0.092	0.388	0.023	0.053	0.058
SCAO 3	0.524	0.058	0.127	0.088	0.511	0.039	0.101	0.083	0.352	0.023	0.049	0.052
SCAO 1	0.447	0.054	0.120	0.077	0.402	0.036	0.090	0.066	0.386	0.023	0.049	0.057
MCAO	0.765	0.574	0.696	0.045	0.736	0.517	0.640	0.051	0.553	0.293	0.385	0.063
GLAO	0.499	0.201	0.342	0.072	0.464	0.158	0298	0.072	0.271	0.094	0.156	0.037
LTAO	0.730	0.135	0.285	0.125	0.710	0.099	0.244	0.124	0.571	0.058	0.127	0.092
SCAO 3	0.689	0.127	0.267	0.117	0.678	0.091	0.226	0.115	0.536	0.051	0.118	0.083
SCAO 1	0.622	0.127	0.247	0.111	0.585	0.090	0.202	0.103	0.536	0.056	0.118	0.084

Table 4: Strehl ratio at J-band (top), H-band (middle) and K-band (bottom) for the different configurations.

	Zenith angle = 0°				Zenith angle = 25°				Zenith angle = 50°			
	Min	Max	Mean	RMS	Min	Max	Mean	RMS	Min	Max	Mean	RMS
MCAO	34.4	41.9	36.4	1.54	34.6	43.1	37.2	1.8	40.2	82.2	52.6	10.0
GLAO	47.1	104.8	70.5	14.5	49.2	128.7	87.9	21.4	92.1	200.0	141.1	24.6
LTAO	39.2	145.6	91.5	29.6	39.9	178.3	116.2	39.7	46.7	246.6	179.4	52.9
SCAO 3	41.5	158.8	99.8	31.8	41.9	192.6	128.7	43.1	50.2	251.9	185.2	52.6
SCAO 1	40.8	158.6	101.4	34.8	48.5	194.6	130.5	41.5	45.3	265.4	181.9	52.6
MCAO	44.5	50.4	46.1	1.25	44.5	51.9	46.6	1.5	47.7	70.4	53.9	4.9
GLAO	51.2	97.0	66.6	10.6	51.8	112.7	71.5	13.8	76.3	162.2	109.3	21.7
LTAO	48.2	119.6	74.6	17.1	48.5	147.3	86.3	26.9	52.2	223.8	141.5	48.8
SCAO 3	49.4	120.6	78.0	18.7	49.5	160.8	92.3	27.8	58,3	200.4	140.9	44.8
SCAO 1	48.2	127.1	82.6	21.5	51.7	173.2	99.7	31.6	53.7	212.7	140.5	44.7
MCAO	59.1	63.2	59.9	0.9	58.8	64.8	60.3	1.3	60.3	75.8	64.4	3.0
GLAO	63.2	98.2	72.6	7.1	63.0	111.9	74.3	9.2	73.0	136.6	92.6	15.0
LTAO	60.8	110.9	76.1	10.7	61.2	137.8	79.8	14.8	64.3	171.9	108.7	30.6
SCAO 3	62.6	112.8	76.8	10.9	62.4	141.4	80.4	14.5	67.2	182.3	110.5	31.4
SCAO 1	62.0	107.2	82.3	13.9	62.2	144.7	89.0	19.9	64.5	168.3	113.0	33.5

Table 5: FWHM at J-band (top), H-band (middle) and K-band (bottom) for the different configurations.

4.3 Multi-conjugate adaptive optics

The Strehl ratio delivered by GNAO in MCAO mode is plotted in Figure 3. The corresponding FWHM is displayed in Figure 4.

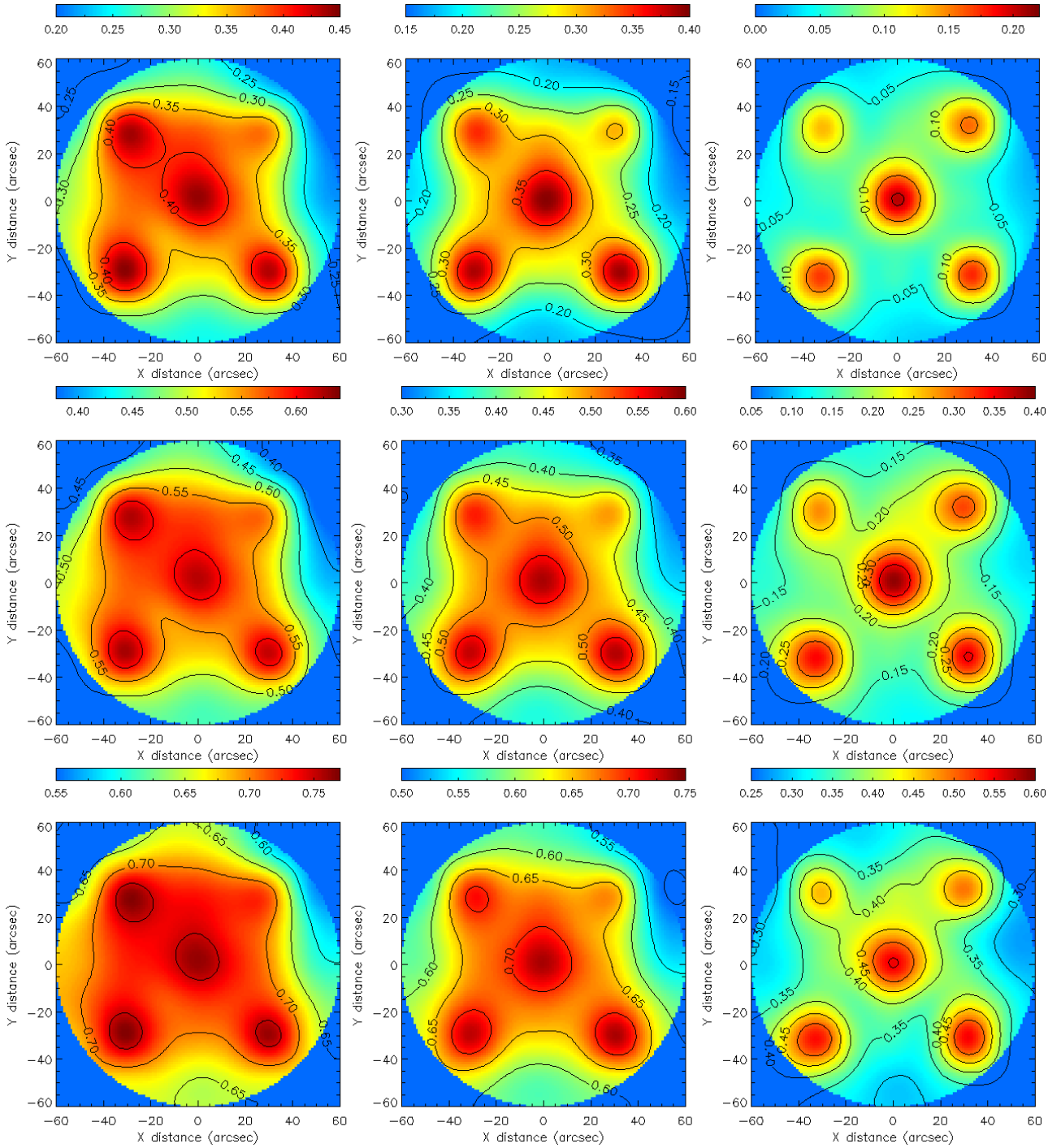

Figure 3: J-band (top), H-band (middle) and K-band (bottom) Strehl ratio as a function of position in the field for zenith angles of 0° (left), 25° (center) and 50° (right) using an MCAO system.

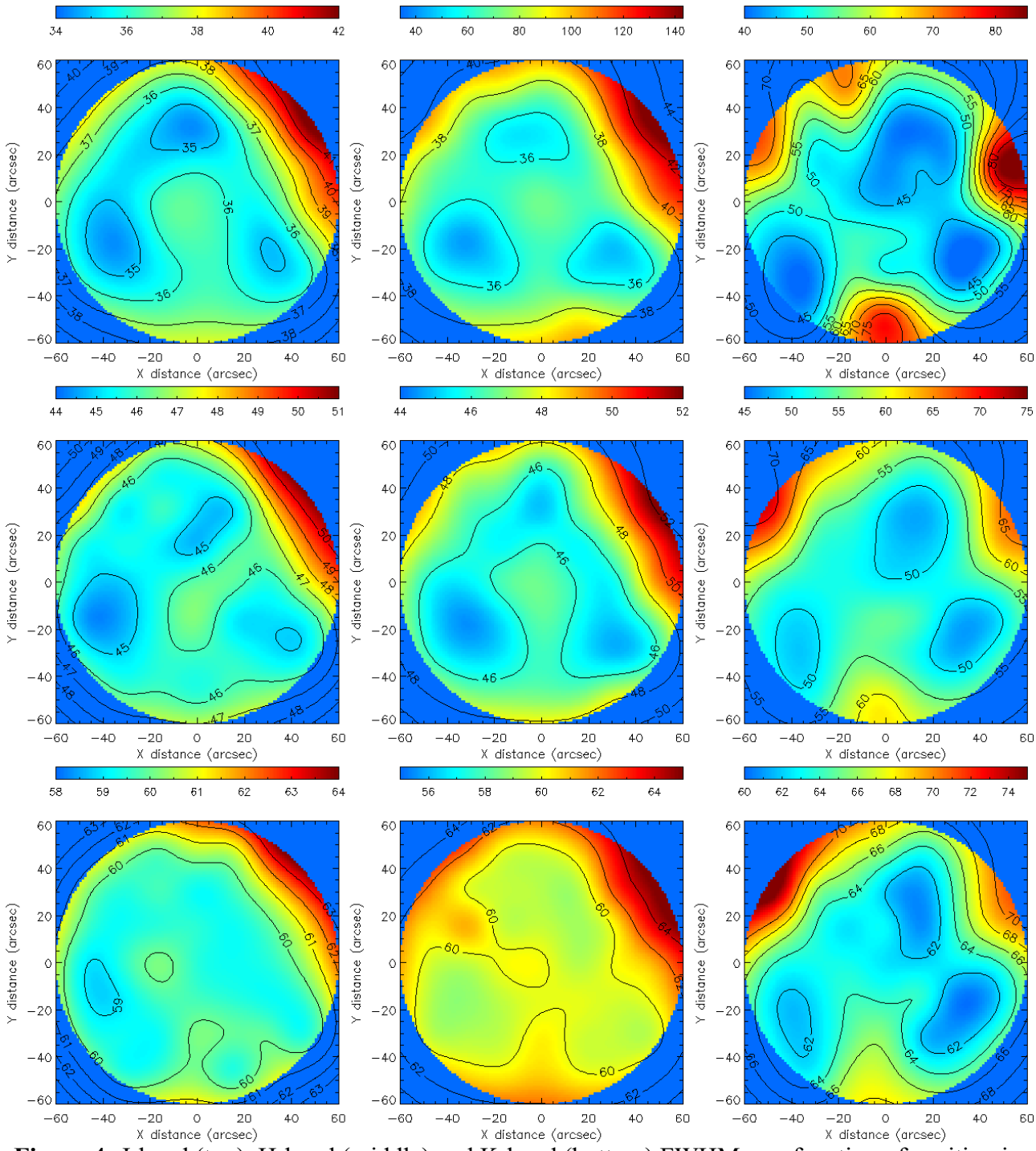

Figure 4: J-band (top), H-band (middle) and K-band (bottom) FWHM as a function of position in the field for zenith angles of 0° (left), 25° (center) and 50° (right) using an MCAO system.

4.4 Ground-layer adaptive optics

The simulation results for the case of ground-layer correction are plotted in Figures 5 and 6.

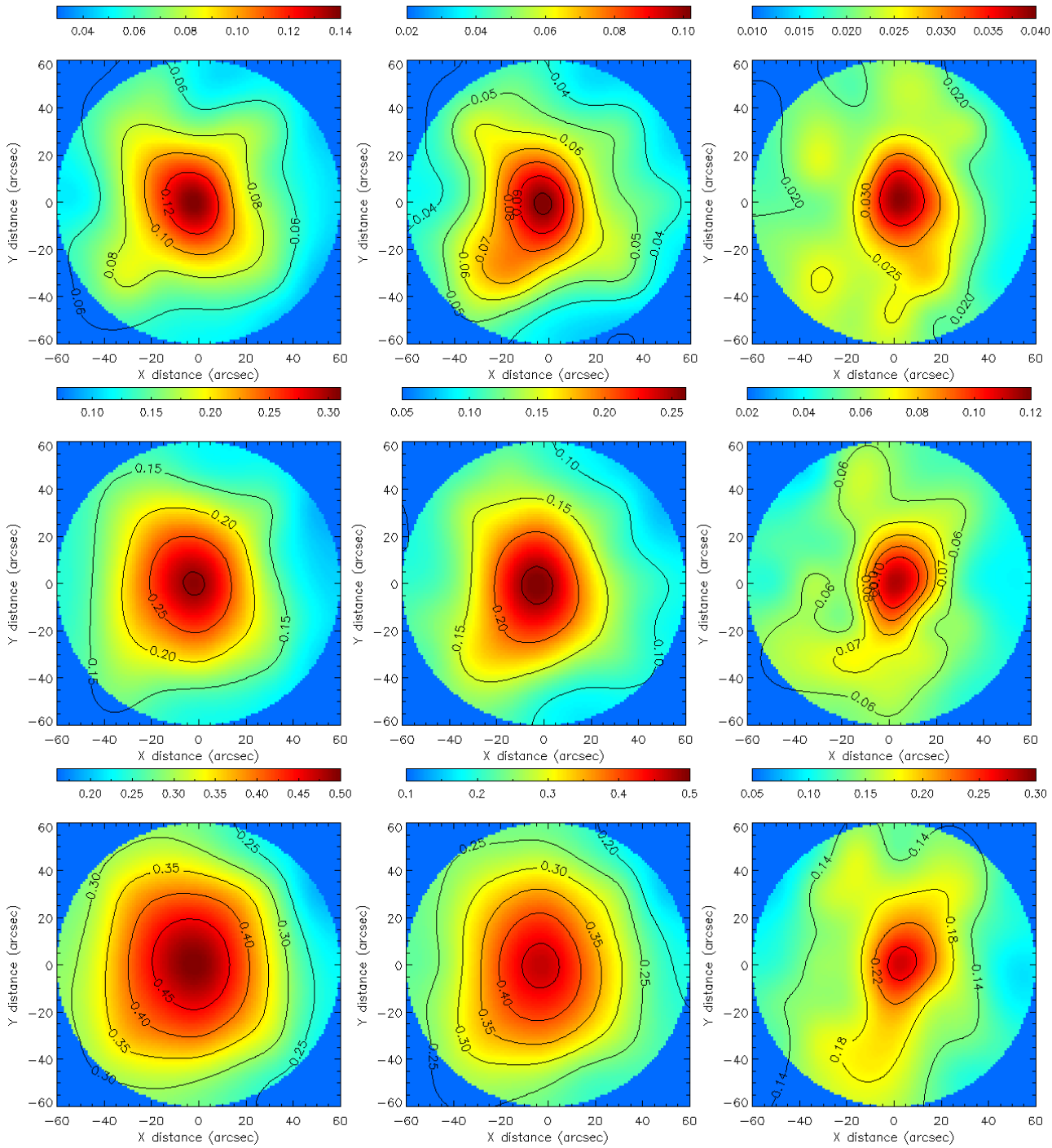

Figure 5: J-band (top), H-band (middle) and K-band (bottom) Strehl ratio as a function of position in the field for zenith angles of 0° (left), 25° (center) and 50° (right) using a GLAO system.

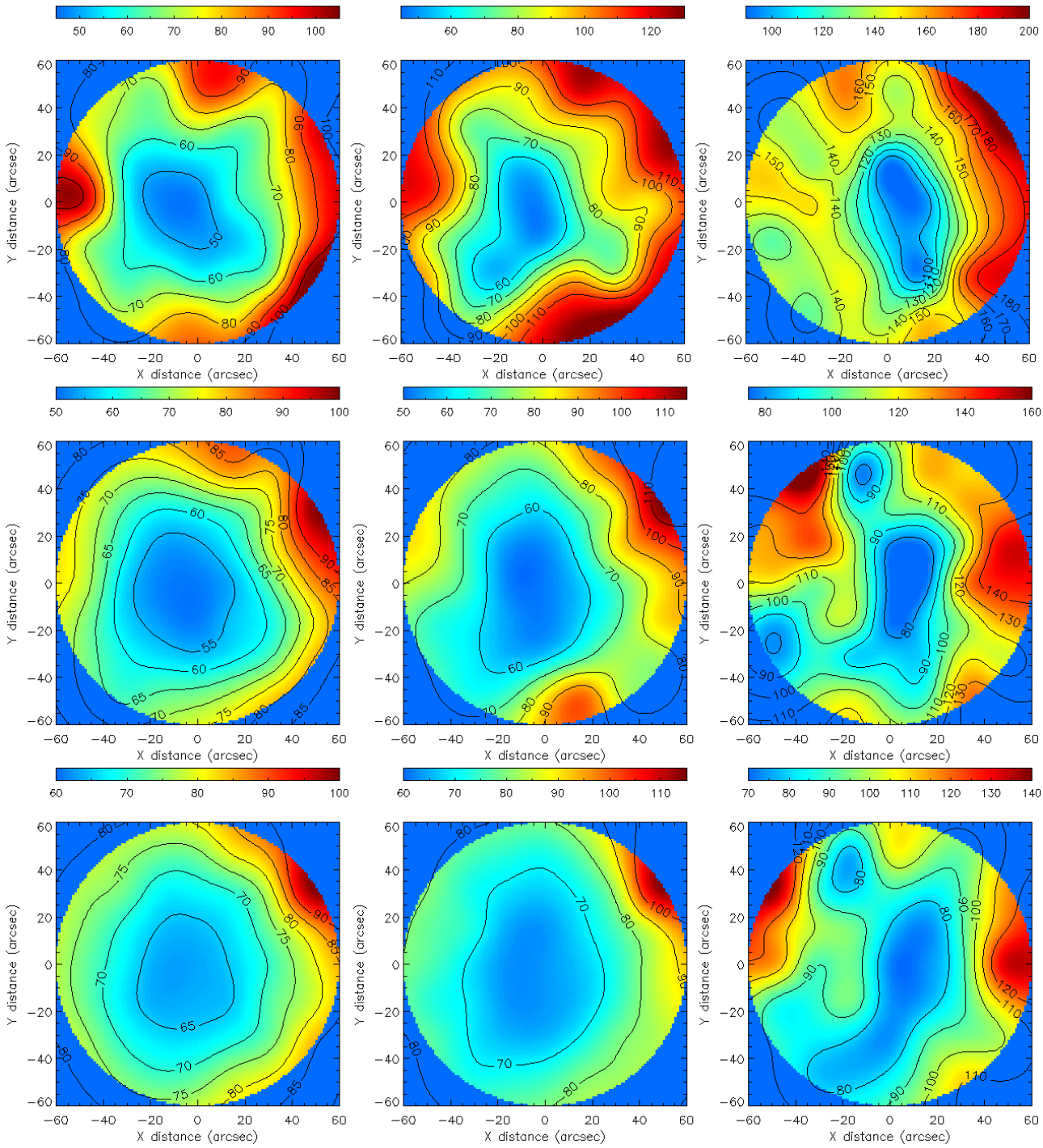

Figure 6: J-band (top), H-band (middle) and K-band (bottom) FWHM as a function of position in the field for zenith angles of 0° (left), 25° (center) and 50° (right) using a GLAO system.

4.5 Laser tomographic adaptive optics

The Strehl and FWHM values from the laser tomography adaptive optics simulations are displayed in Figures 7 and 8.

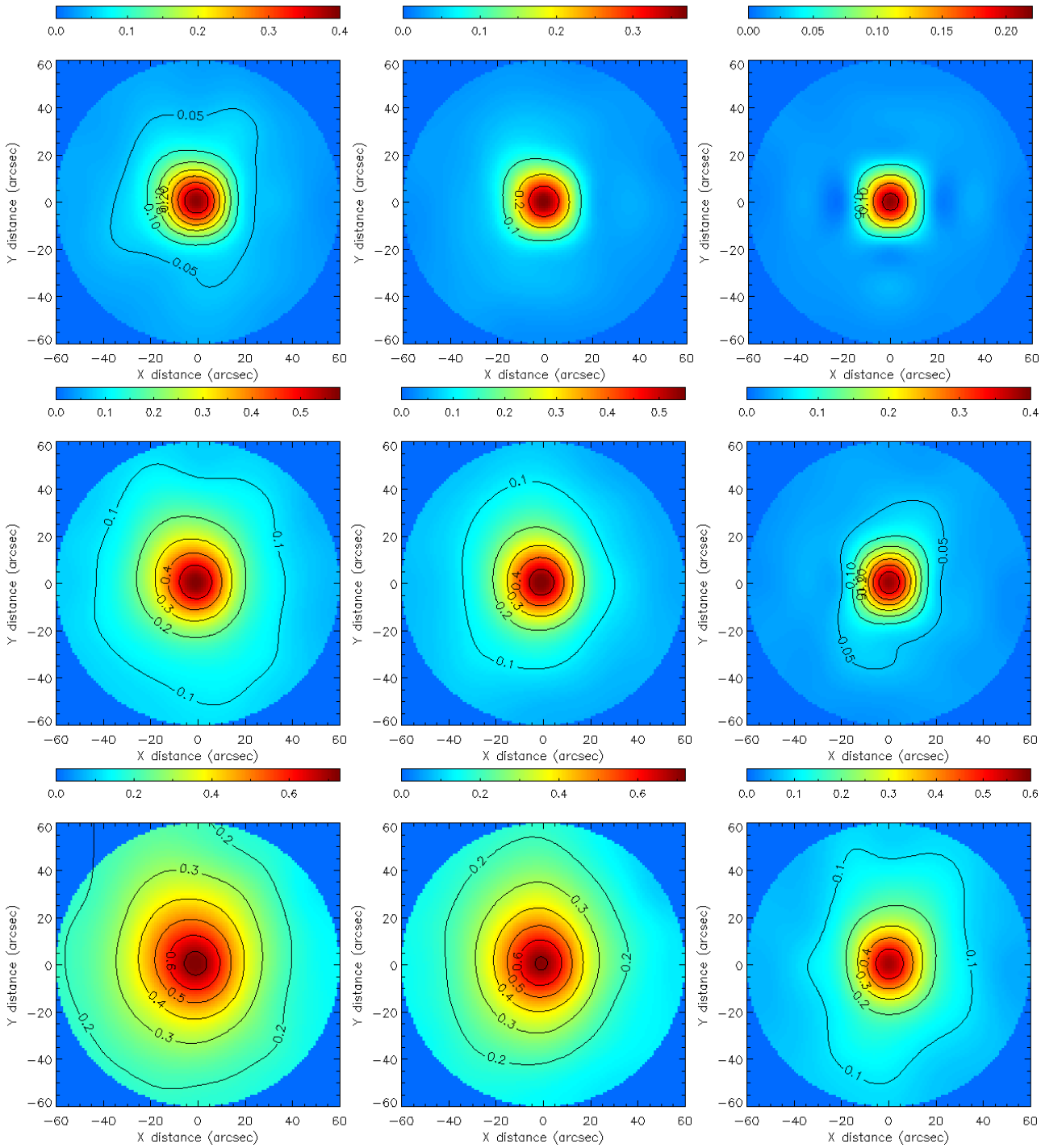

Figure 7: J-band (top), H-band (middle) and K-band (bottom) Strehl ratio as a function of position in the field for zenith angles of 0° (left), 25° (center) and 50° (right) using an LTAO system.

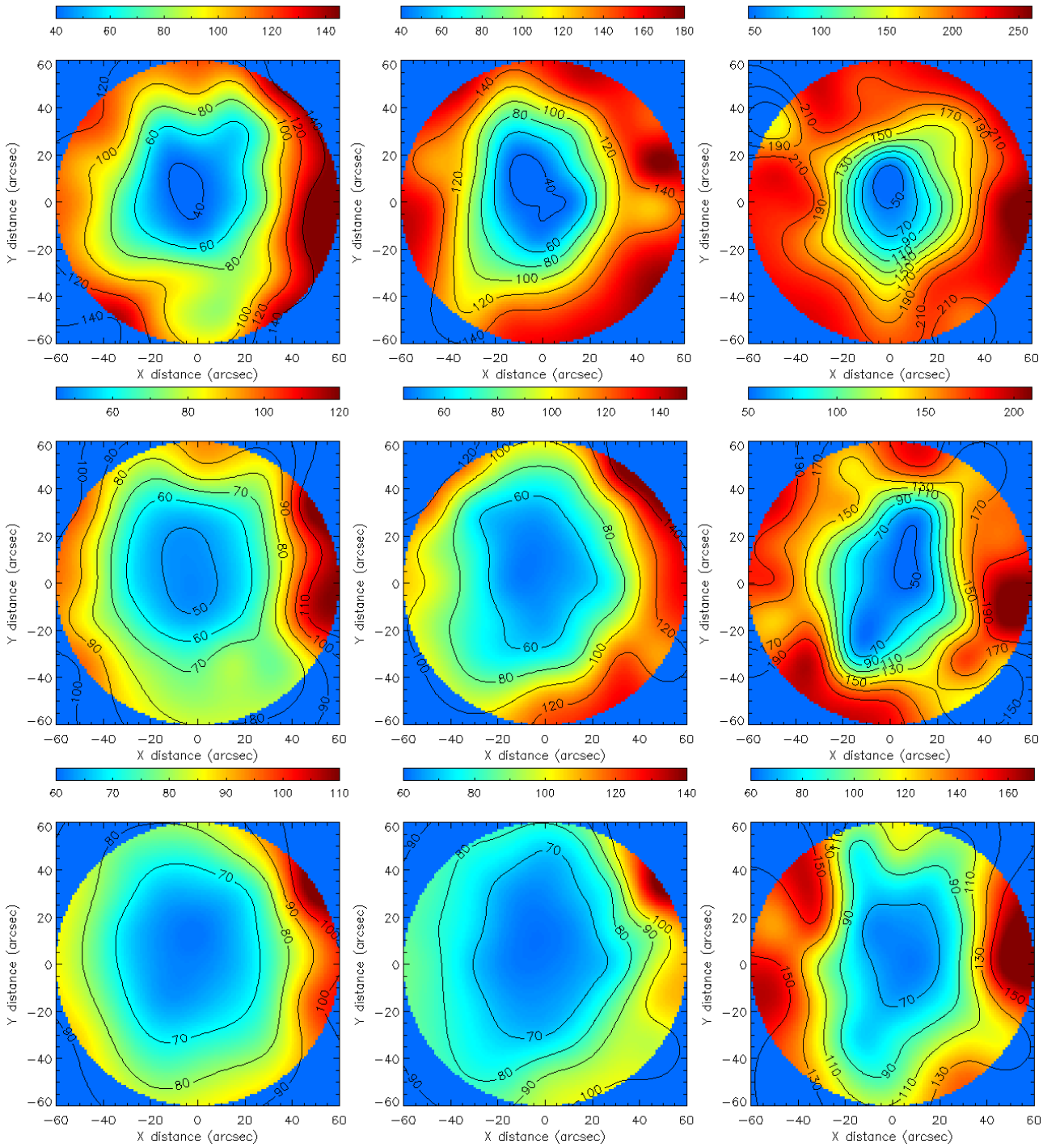

Figure 8: J-band (top), H-band (middle) and K-band (bottom) FWHM as a function of position in the field for zenith angles of 0° (left), 25° (center) and 50° (right) using an LTAO system.

4.6 Single conjugate adaptive optics (3 NGS)

Figures 9 and 10 show the results of the single conjugate adaptive optics system with three NGSs.

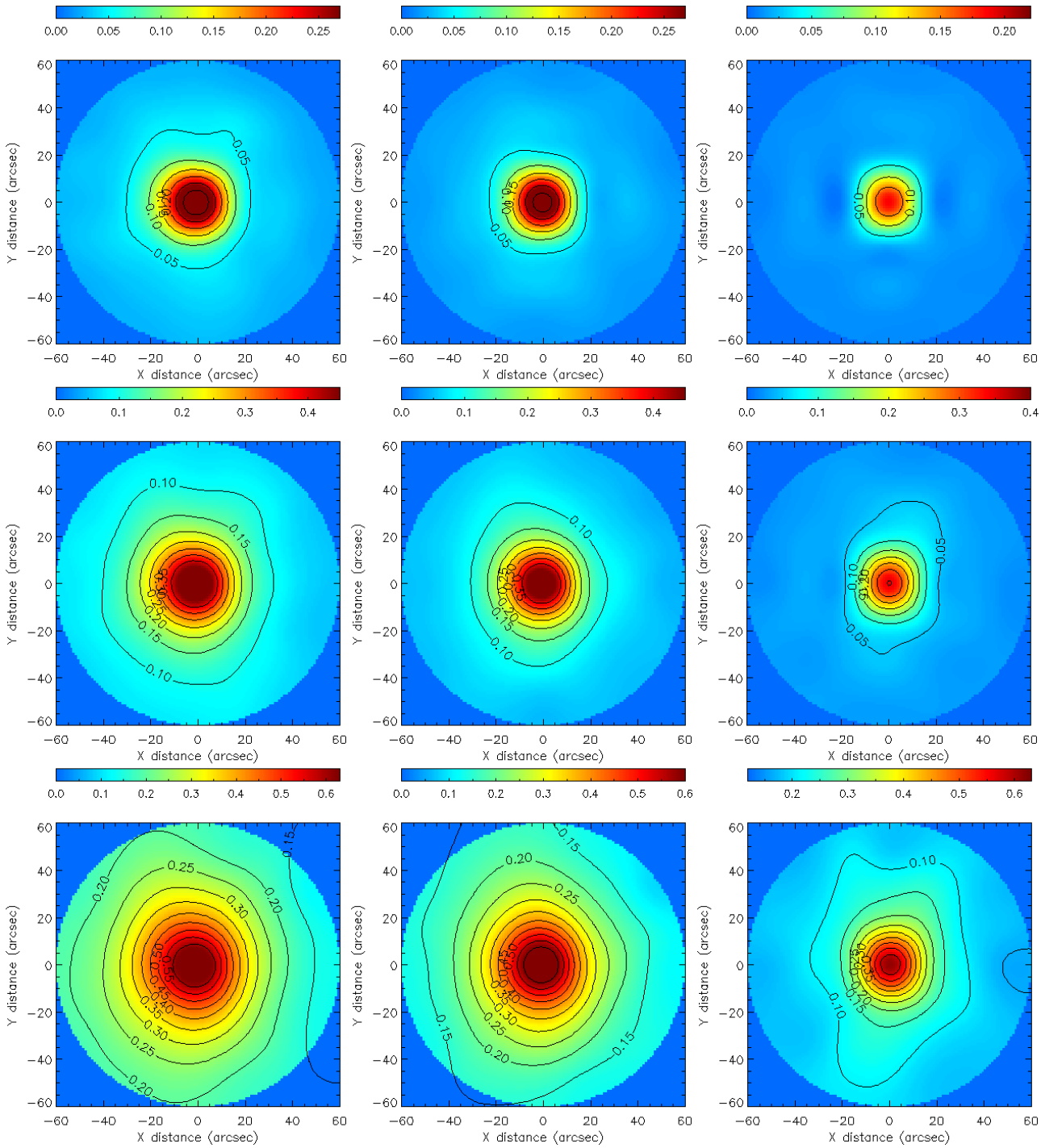

Figure 9: J-band (top), H-band (middle) and K-band (bottom) Strehl ratio as a function of position in the field for zenith angles of 0° (left), 25° (center) and 50° (right) using an SCAO system with three NGSs.

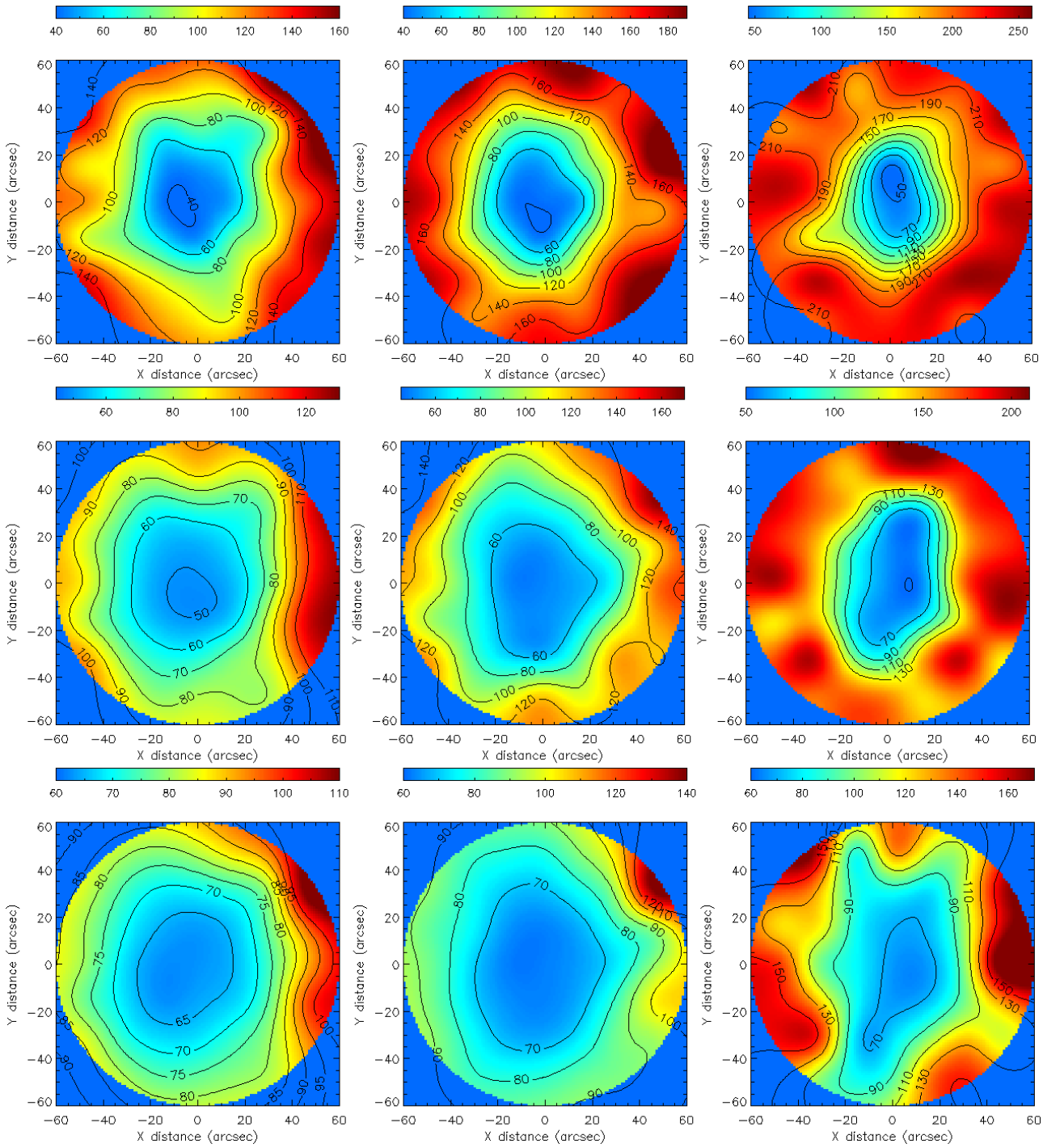

Figure 10: J-band (top), H-band (middle) and K-band (bottom) FWHM as a function of position in the field for zenith angles of 0° (left), 25° (center) and 50° (right) using an SCAO system with three NGSs.

4.7 Single conjugate adaptive optics (1 NGS)

The results of the classical LGS AO simulations with a single NGS are plotted in Figures 11 and 12.

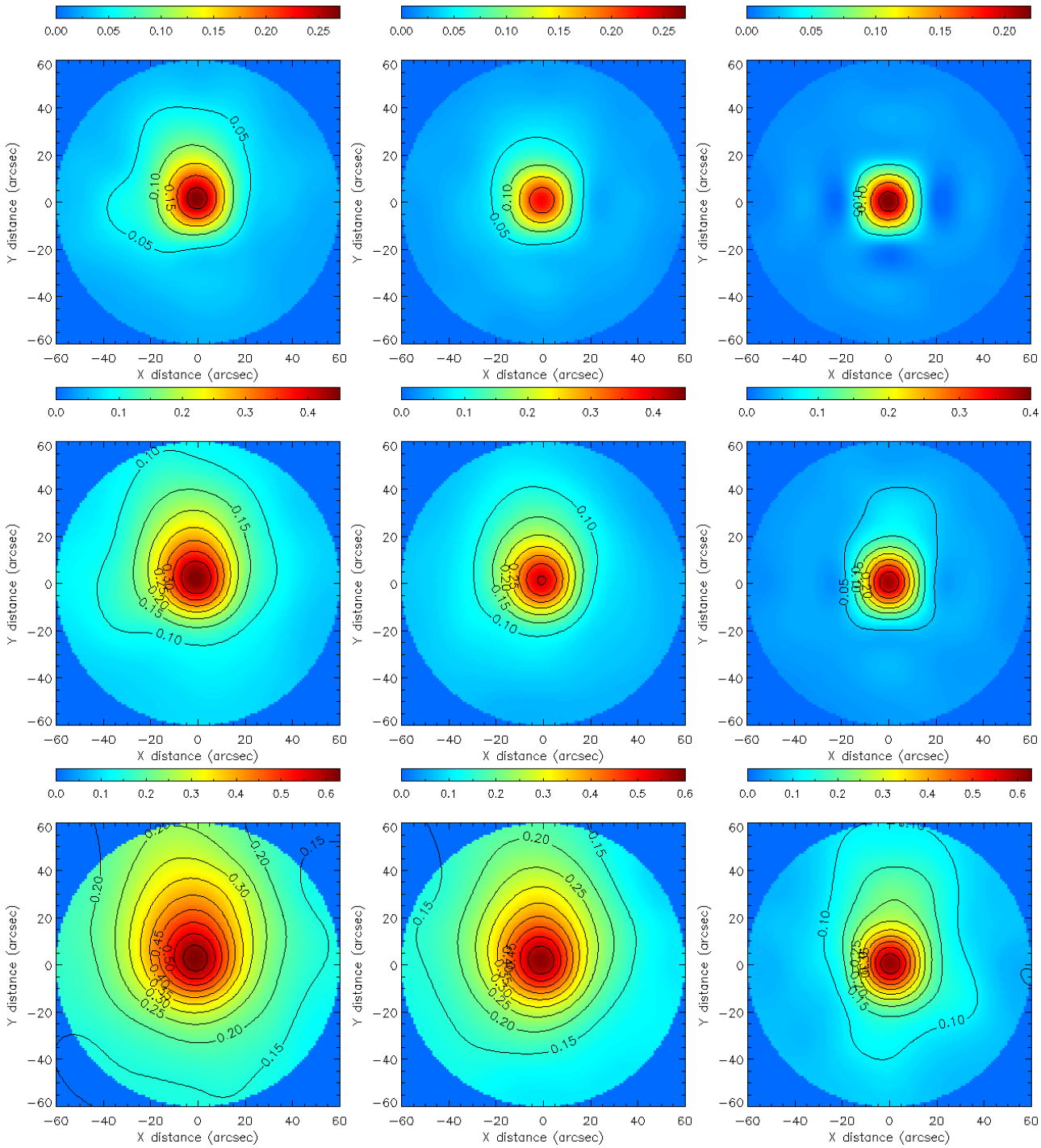

Figure 11: J-band (top), H-band (middle) and K-band (bottom) Strehl ratio as a function of position in the field for zenith angles of 0° (left), 25° (center) and 50° (right) using an SCAO system with one NGS.

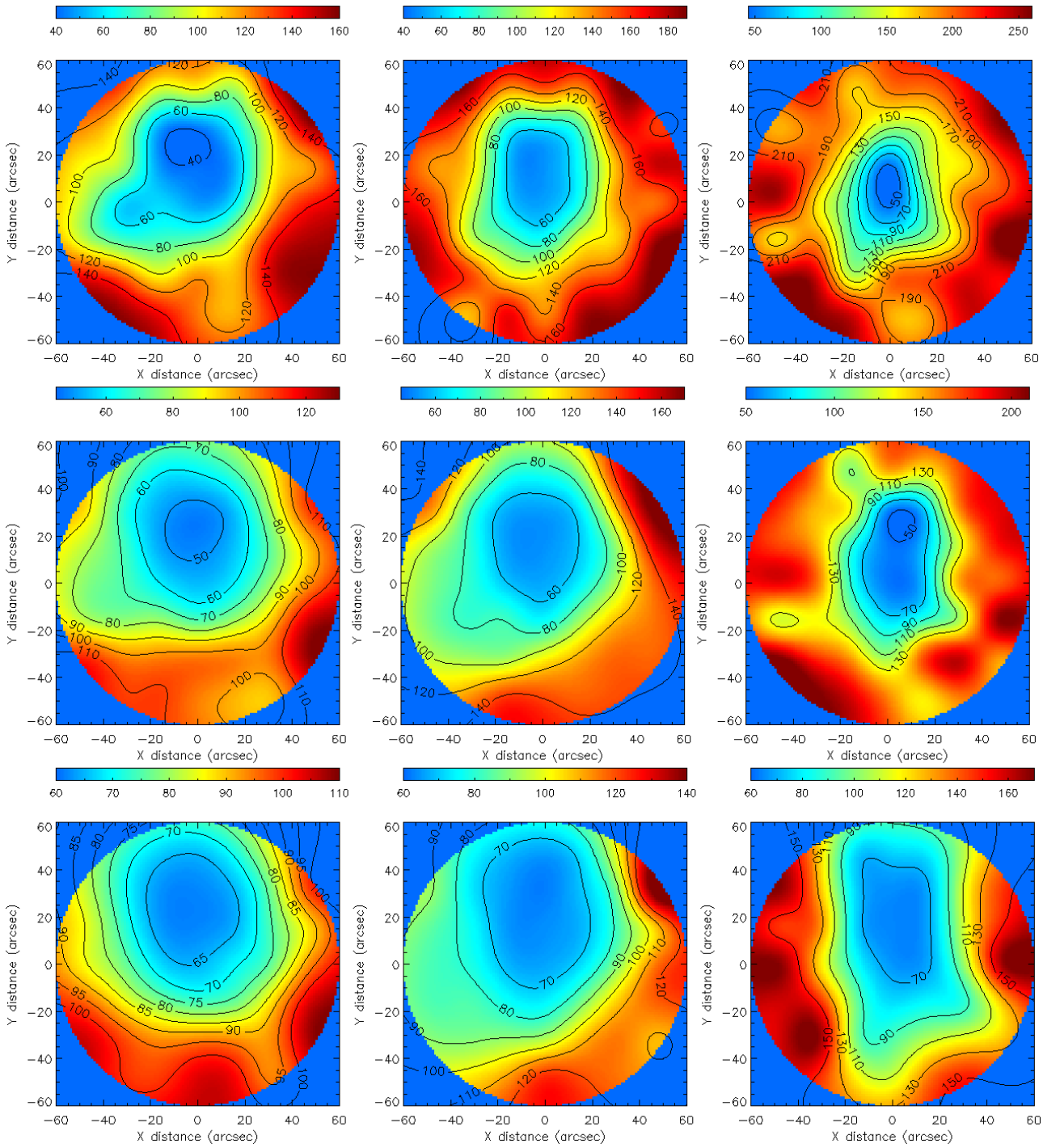

Figure 12: J-band (top), H-band (middle) and K-band (bottom) FWHM as a function of position in the field for zenith angles of 0° (left), 25° (center) and 50° (right) using an SCAO system with one NGS.